Phase separation of passive particles in active liquids

Pragya Kushwaha [1], Vivek Semwal,[2] Sayan Maity,[1] Shradha Mishra,[2] and Vijayakumar Chikkadi [1]

[1]*Indian Institute of Science Education and Research, Pune 411008, India*
[2]*Indian Institute of Technology (BHU), Varanasi 221005, India*

The transport properties of colloidal particles in active liquids have been studied extensively. It has led to a deeper understanding of the interactions between passive and active particles. However, the phase behavior of colloidal particles in active media has received little attention. Here, we present a combined experimental and numerical investigation of passive colloids dispersed in suspensions of active particles. Our study reveals dynamic clustering of colloids in active media due to an interplay of activity and attractive effective potential between the colloids. The strength of the effective potential is set by the size ratio of passive particles to the active ones. As the relative size of the passive particles increases, the effective potential becomes stronger and the average size of the clusters grows. The simulations reveal a macroscopic phase separation at sufficiently large size ratios. We will discuss the effect of density fluctuations of active particles on the nature of effective interactions between passive ones.

I. INTRODUCTION

The Brownian colloids self-assemble to display a wide variety of phases depending on their shapes and interactions [1–3]. Their equilibrium phase behavior is governed by the principles of equilibrium statistical mechanics [4,5]. However, our understanding of the collective behavior of colloids far from equilibrium remains a challenge [6,7]. In recent years, active matter has emerged as a new paradigm for understanding nonequilibrium systems [8–11]. They are known to display many interesting phenomena such as flocking [12,13], motility-induced phase separation [14–16], active turbulence [17], and superfluidity [18], which are absent in equilibrium systems. Therefore, active matter offers novel approaches to colloidal assembly in systems far from equilibrium. In this article, we have investigated the phase behavior of colloidal particles dispersed in active liquids.

Wu and Libchaber [19] did seminal experiments on the active transport of colloidal particles in suspensions of bacteria. They discovered anomalous diffusion and a large effective diffusion constant, when compared to diffusion at equilibrium, which inspired a slew of theoretical investigations and detailed experiments [20–27]. The subsequent efforts have elucidated how enhanced diffusion arises due to an interplay of entrainment of colloids by bacteria, far-field hydrodynamic interactions, direct collisions, and the relative size of bacteria and colloids [23–25]. Further, the effective interaction between a pair of passive particles in active media has been predicted to be attractive, repulsive, and long ranged, depending on the geometry of passive particles, the activity of active species, and their density [28–36]. This understanding has opened new routes to colloidal assembly mediated by active fluids [7,37].

The phase behavior of active-passive mixtures is a topic of recent interest [11,37–45], where experimental investigations

are scarce [6,7]. On the one hand, theory and simulations at high Peclet numbers have shown that homogeneous mixtures of active and passive particles are unstable. The underlying physics is similar to motility-induced phase separation [40,42]. On the other hand, in the diffusive limit, theory and simulations of nonequilibrium binary mixtures with different diffusivities and temperatures reveal phase separation [41,44,46] due to spinodal-like instability. Surprisingly, there is little known about mixtures at moderate Peclet numbers. This is the range where most of the active matter experiments involving living matter or synthetic systems, such as diffusiophoretic colloids, fall. A recent study of colloids in active suspensions of bacteria in experiments and simulations reports dynamical clustering of colloids at moderate Peclet numbers [6]. The clustering was shown to be stabilized by the torque on active particles, which align their velocities tangential to the surface of colloids, leading to microphase separation. The experiments were conducted over a range of densities of bacteria, while the simulations were performed over a range of Peclet numbers and torques of active particles to describe their phase behavior. However, the nonequilibrium steady states of the system are dependent on several other parameters, such as the size ratio of colloids to bacteria, density of colloidal particles, and the hydrodynamics interactions, and our understanding of these aspects in active-passive matter is far from complete. Here we present a combined experimental and numerical study of the phase behavior of colloidal particles in active media, with a focus on the effect of size ratio on the phase behavior and the role of density fluctuations of active particles in mediating effective interactions between passive ones. Our investigations are motivated by the well-studied system of colloid-polymer mixture [47,48], where the equilibrium phase diagram is determined by the competition between thermal fluctuations and effective interaction that are dependent on multiple parameters such as size ratio, polymer concentration, and density of colloids.
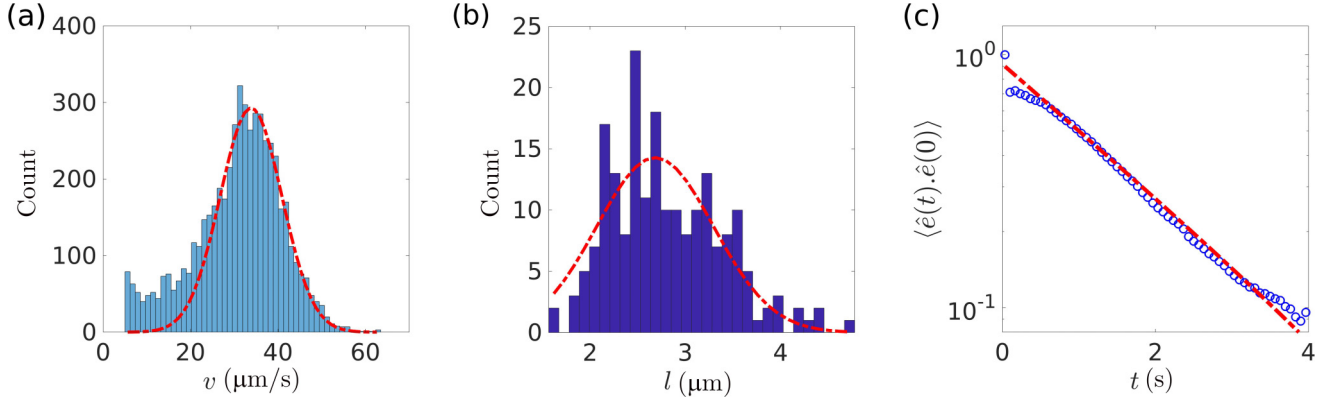
FIG. 1. (a) Histogram of bacteria velocities. The average velocity is $\langle v \rangle = 33.84 \pm 9.98$ μm/s. (b) Histogram of the size of the bacteria. The size of the bacteria is its length along the longer axis. The average length of the cells is $\langle l \rangle = 2.68 \pm 0.86$ μm. (c) The rotational diffusion time of the bacteria was estimated from their normalized velocity autocorrelation function. The dashed line is an exponential fit to the data, which gives a rotational diffusion time of $\tau_r \sim 1.67$ s.

II. EXPERIMENTAL SYSTEM AND SIMULATIONS MODEL

A. Experimental method

The active-passive mixtures in experiments are realized using large colloidal particles and suspensions of motile bacteria. We have used polystyrene colloids of sizes ranging from 5 to 15 μm, which were purchased from MicroParticles, GmBH, Germany. The active suspensions were prepared using *Escherichia coli* cells (U5/41 type strain). The cells were cultured using well-established protocols in the literature [18,49]. They were grown overnight at $37\,°C$ in a Luria Bertani (LB) agar plate containing 1% tryptone, 1% NaCl, 0.5% yeast extract, and 1.5% agar. A single colony of *E. coli* was added to 10 ml of LB broth and kept at $37\,°C$ until OD_{600} (optical density at 600 nm wavelength) reached a value of 1.3. Bacterial cells were then harvested and washed three times with motility media (10 mM potassium phosphate (*p*H 7.0), 0.1 mM EDTA, 0.002% Tween-20, and 5 mM L-serine) by centrifugation at 3000 rpm for 5 min at room temperature to remove the traces of LB broth. The pellet was later resuspended in motility media to get desired concentrations. The observation chamber was created using a circular cavity of size 1 cm and 100 μm deep, which was glued to a polyethylene glycol (PEG)-coated coverslip using double-sided tape. The bacteria density of the sample with $OD_{600} = 1$ was estimated to contain 6×10^9 cells/ml (b_0). The density of bacteria in our experiments was fixed at $10b_0$, which was well below the density threshold for the onset of collective motion.

Figures 1(a)–1(c) show the distribution of speeds and sizes, and the autocorrelations of cell orientations, respectively, measured using a dilute suspension of cells. The average speed of the cells is $v = 33.84 \pm 9.98$ μm/s and their average size is $l = 2.68 \pm 0.86$ μm. The rotational diffusion timescale was estimated to be $\tau_r \sim 1.67$ s. The Peclet number, which is defined as $Pe = \tau_r v / l$, turns out to be $Pe \sim 21$ for our system. The phase behavior of colloidal particles in suspensions of bacteria was investigated by varying the size and density of the beads at a constant density of bacteria. The diameters of the particles used in the experiments were $\sigma = 7$, 10, and 15 μm, and their density is varied from

$\phi \sim 0.1$–0.4, where $\phi = N\pi\sigma^2/(4A)$ is the area fraction and N is the number of colloidal particles in the field of view of area A. The size ratio $S = \sigma/l$ is defined as the ratio of the diameter of colloids to the length of the bacteria.

B. Simulation method

The simulations were performed using a binary mixture of active Brownian particles (ABPs) with N_a small active particles of radius a_a and N_p big passive particles of radius a_p ($a_p > a_a$) moving on a two-dimensional frictional substrate. The active particles are associated with a self-propulsion speed v and an orientation unit vector $\mathbf{v}_i = (\cos\theta_i; \sin\theta_i)$, where θ_i is the angle between the velocity vector and a reference direction [50–52]. The motion of ABPs is governed by the following Langevin equations:

$$\frac{d\mathbf{r}_i}{dt} = v\mathbf{v}_i - \mu_1 \sum_{j \neq i} \mathbf{F}_{ij} + \sqrt{2D_T}\boldsymbol{\eta}_{Ti}, \qquad (1)$$

$$\frac{d\theta_i}{dt} = \Gamma \sum_i \sin(\theta_i - \theta_{ij}) + \sqrt{2D_r}\eta_{ri}. \qquad (2)$$

Here μ_1 is the mobility and $\mathbf{F}_{ij}$ is the force acting on particle i due to particle j. The noise term is defined as $\langle \eta_{r,Ti}(t)\eta_{r,Tj}(t')\rangle = 2D_{r,T}\delta_{ij}\delta(t-t')$, D_T and D_r are the translational and rotational diffusion constants of active particles and Γ is the magnitude of torque that aligns the velocity vector of active particles tangential to the surface of passive particles [27], and $\theta_{ij} = \arg(\mathbf{r}_i - \mathbf{r}_j)$. The persistence length $l_p = v/D_r$ of active particles is constant in our simulations; it is set at $l_p = 20a_a$. The other constants in our simulations are $D_T = 0.005$ and $\Gamma = 1$.

The equation of motion for passive particles is

$$\frac{d\mathbf{r}_i}{dt} = \mu_2 \sum_{j \neq i} \mathbf{F}_{ij}, \qquad (3)$$

where μ_2 is the mobility of passive particles. There is no translational noise in Eq. (3), so the dynamics of passive particles is only due to interaction force. We choose the mobility of both species to be the same, i.e., $\mu_1 = \mu_2 = \mu$. Particles interact through short-ranged soft repulsive forces $\mathbf{F}_{ij} = F_{ij}\hat{\mathbf{r}}_{ij}$, where
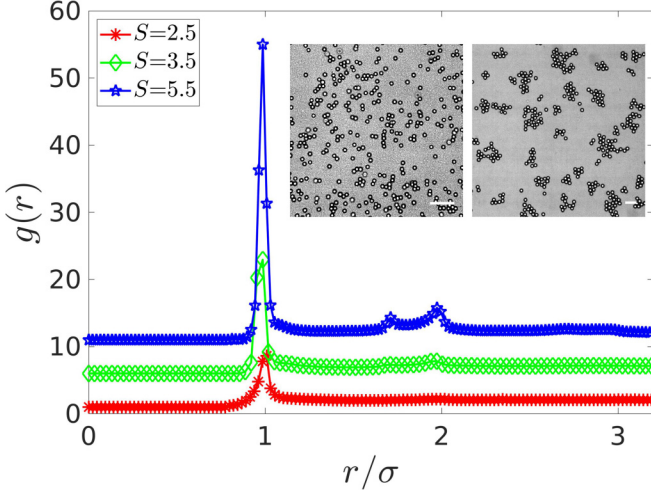
FIG. 2. The structure of colloidal clusters in active liquids. Main panel: The pair correlation function $g(r)$ for $\phi \sim 0.10$ and $S \sim 2.5$, 3.5, and 5.5. The $g(r)$ curves are shifted along the y axis for clarity. Insets: The bright-field images of particles at $\phi \sim 0.10$ and size ratios $S \sim 2.5$ (left) and $S \sim 5.5$ (right), respectively. The scale bar in the images is 50 μm.

$F_{ij} = k(a_i + a_j - r_{ij})$ when $r_{ij} \leqslant (a_i + a_j)$ and $F_{ij} = 0$ otherwise; $r_{ij} = |r_i - r_j|$ and k is a constant. The elastic timescale in our system is defined by $(\mu k)^{-1} = (150)^{-1}$.

We simulate the system in a square box of length l_{box}, with periodic boundary conditions. The system is defined by the area fractions $\phi_a = N_a \pi a_a^2 / l_{\text{box}}^2$ and $\phi_p = N_p \pi a_p^2 / l_{\text{box}}^2$ of the active and passive particles, respectively, the activity v of active particles, and the size ratio ($S = a_p/a_a$) defined as the ratio of the radius of a passive particle to the radius of an active particle. A random homogeneous distribution of active and passive particles in the box and with random directions for the velocity of active particles are the initial conditions in simulations. Equations (1)–(3) are updated for all particles and one simulation step is counted after a single update for all the particles. The simulation does not include the hydrodynamic interactions that are present in experiments. The effect of a hydrodynamic interaction can be included using coarse-grained studies similar to [53].

III. EXPERIMENTAL RESULTS

Dynamic clusters of colloids in active liquids and the effect of size ratio

We first present the experimental results. The colloids used in our experiments are non-Brownian as they are bigger than 5 μm. However, they diffuse in suspensions of bacteria due to active fluctuations with a characteristic superdiffusive motion on short timescales and a diffusive motion on long timescales. To investigate their collective behavior in active suspensions, we first analyze their pair correlation function $g(r)$, which is shown in the main panel of Fig. 2 at an area fraction of $\phi \sim 0.1$ and size ratios $S \sim 2.5$–5.5. The normalized $g(r)$ for different size ratios is shifted along the y axis for clarity. What is prominent is the presence of a sharp peak at $r = \sigma$, and additional peaks develop at $r = 1.7\sigma$ and $r = 2\sigma$ with

increasing size ratio. The peak at 2σ indicates a second shell of neighbors, and the one at 1.7σ is a signature of hexagonal ordering in the cluster. These observations are evident in the bright-field images presented in the insets of Fig 2. The larger size ratios lead to larger clusters with enhanced order. These images are reminiscent of clustering in systems of purely active particles [15]. However, the clusters of passive particles in our experiments break and form much more rapidly. A real-time video of dynamic cluster formation is presented in the Supplemental Material video SV1 for $\phi \sim 0.10$ and $S \sim 2.5$ [54]. Recent simulations have reported similar dynamic clustering and traveling interfaces of active-passive particles that are not observed in our current study [40,42]. One of the main differences between our experiments and these simulations is the large Peclet numbers used in simulations. Further, as reported by earlier investigations, clustering is a manifestation of an attractive effective potential between the passive particles due to active fluctuations [28].

We next turn our attention to cluster size distribution (CSD), $p(n)$, which is a count of clusters of n particles [43,55]. The clusters in our experiments were determined by setting a distance criterion of $r_c \leqslant 1.1\sigma$ to identify pairs of particles as neighbors. This was set based on the position of the first peak of $g(r)$ in Fig. 2, and to account for small polydispersity ($<5\%$) in the size distribution of colloidal particles. The results of our analysis are presented in Figs. 3(a) and 3(b). The main panel in Fig. 3(a) shows the CSD for varying size ratios of $S \sim 2.5$, 3.5, and 5.5 at a density of $\phi \sim 0.1$. For small size ratios $S < 5$, $p(n)$ has an exponential form $\exp(-n/n_0)$ as observed in the equilibrium case [52]. The clustering is weak at these size ratios; however, for $S > 5$ the $p(n)$ displays a power-law decay with an exponential cutoff at large n, i.e., it is best described by $p(n)/p(1) \sim 1/n^\alpha \exp(-n/n_0)$. The fits of this form to our data are shown in the figure using dashed lines. The value of α varies with the area fraction ϕ of colloids. It takes values from $\alpha \sim 0.57$ at $\phi \sim 0.1$ to $\alpha \sim 1.3$ at $\phi \sim 0.4$. These results indicate that the characteristic size of clusters grows with increasing size ratio. The growth of clusters is dramatic at larger area fractions; the inset of Fig. 3(a) shows cluster distribution at $\phi \sim 0.3$. We further elucidate the clustering of colloids by computing the average cluster size using the expression $\langle n \rangle = \sum n p(n)$, which is presented in Fig. 3(b) where the curves with different symbols correspond to different area fractions ranging from $\phi \sim 0.1$ to 0.4. These measurements were made in the steady state. What is clear from Fig. 3(b) is that increasing the size ratio or the relative size of colloids leads to larger cluster sizes. This suggests that the effective potential between the colloids becomes stronger with an increasing size ratio. One can intuitively understand the underlying physics by considering the interaction between an isolated colloidal particle and a swimmer. When the size of a particle is small, bacterium entrains the particle to larger distances before changing its direction of motion. However, when the particle is large, the entrainment distance is small, and the scattering angle of the swimmer is large [25]. It indicates that the bacteria can suppress cluster formation when the colloidal particles are smaller. What is not clear from our experiments is whether larger size ratios lead to a macroscopic phase separation in our system. To understand this aspect, we turn to numerical simulations that allow a detailed exploration of parameter space.
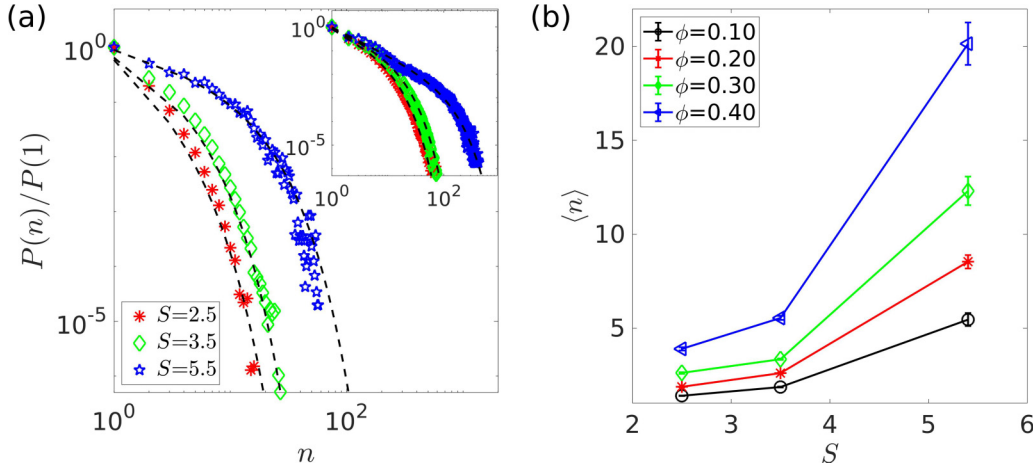
FIG. 3. Size of colloidal clusters and the effect of size ratio. (a) Cluster size distribution in the main panel is shown for different size ratios $S \sim 2.5, 3.5,$ and 5.5 at a density of $\phi \sim 0.10$. The symbols distinguish different size ratios. The inset shows the CSD plot for same size ratios at $\phi \sim 0.3$. (b) The average cluster size $\langle n \rangle$ for varying S. The curves with different symbols correspond to different particle densities, ranging from $\phi \sim 0.1$–0.4.

IV. SIMULATION RESULTS

A. Effective potential between a pair of ABPs in active media

We turn to simulations in order to understand the experimental observations. We first investigate the effective potential between a pair of ABPs in active media in our simulations. Consider two passive particles with their positions at $\mathbf{r}_1$ and $\mathbf{r}_2$ in a system of ABPs with $N_a = 1800$, corresponding to an ABP area fraction of $\phi_a = 0.5$. The position of the first particle at $\mathbf{r}_1$ is fixed, while the position of the second particle is slowly varied in small steps of $\Delta x = 0.5 a_a$ starting from the zero surface to surface distance between two passive particles. The cartoon of the system simulated for the force calculation for a fixed r is shown in the top inset of Fig. 4. The ABPs are shown in red and passive particles in blue for $S = 8$. For resolution, only a part of the system near the two passive particles is shown. The active particles' positions and orientations are updated according to the Eqs. (1) and (2). For each configuration at a given distance between two passive particles, the system is allowed to reach the steady state. Further, we use the steady-state configuration to calculate the force $\mathcal{F}^S(r)$ between two passive particles at a surface to surface separation r, such that $\mathcal{F}^S(r) = \mathbf{F}_{12}(r) + \sum_{i=1}^{N_a} \mathbf{F}_{1i}(r)$. Here $\mathbf{F}_{12}(r)$ is the force due to passive particle second on first, and $\sum_{i=1}^{N_a} \mathbf{F}_{1i}(r)$ represents the sum of all the forces due to active particles on the first passive particle for a given configuration of two passive particles at separation r. The potential is then calculated by integrating the force over the distance $U(r) = \int_{-\infty}^{r} \mathcal{F}^S(r) dr$ [56–58]. Here we set the lower limit as one-fourth of the box length. The results are averaged over 30 independent realizations.

The main panel in Fig. 4 shows the effective potentials $U(r)$ computed at $Pe = 25$ and four size ratios $S = 3, 5, 8,$ and 10, which are comparable to experimental values. The distance is normalized by the radius of active particles, which is kept fixed to 0.1. The negative side of the potential shows attraction and the positive nature is repulsion. For all the parameters the potential approaches zero at large distances, and it is negative at intermediate distances. The depth of the

potential becomes deeper with increasing S. The inset shows the effective potential with the distance r scaled by the size of passive particles. Surprisingly, the minima of the potentials for the size ratios $S = 5, 8,$ and 10 fall at $r/a_p = 1$, which implies that the length scale characterizing the range of the interaction potential is set by the size of passive particles.

B. Density fluctuations of active particles

The interactions between passive particles in simulations are primarily mediated by active particles. Naturally, their
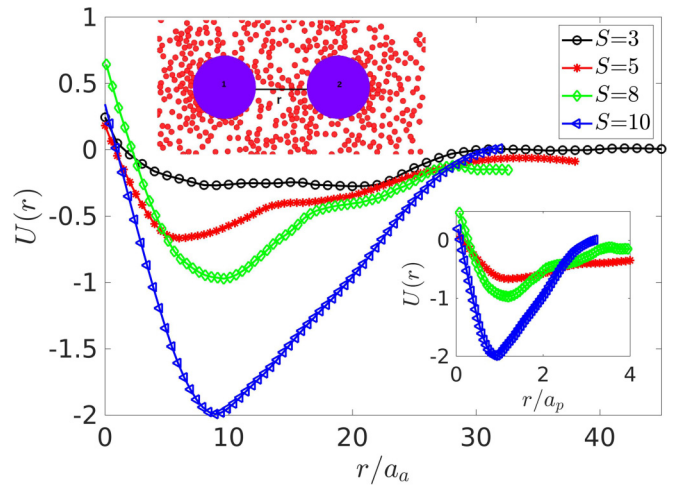

FIG. 4. The effective potential between a pair of colloidal particles. The main panel shows the plot of the effective potential $U(r)$ vs scaled distance r/a_a for $Pe = 25$ and size ratios $S = 3, 5, 8,$ and 10. The top inset shows a snapshot of the part of the system used to calculate the potential. The two bigger particles are passive particles with the left one marked as particle 1 and the right one marked 2 with positions $\mathbf{r}_1$ and $\mathbf{r}_2$, respectively. The red circles are ABPs. The line shows the surface to surface distance r between two passive particles. The bottom inset shows the effective potential with the scaled distance r/a_p.
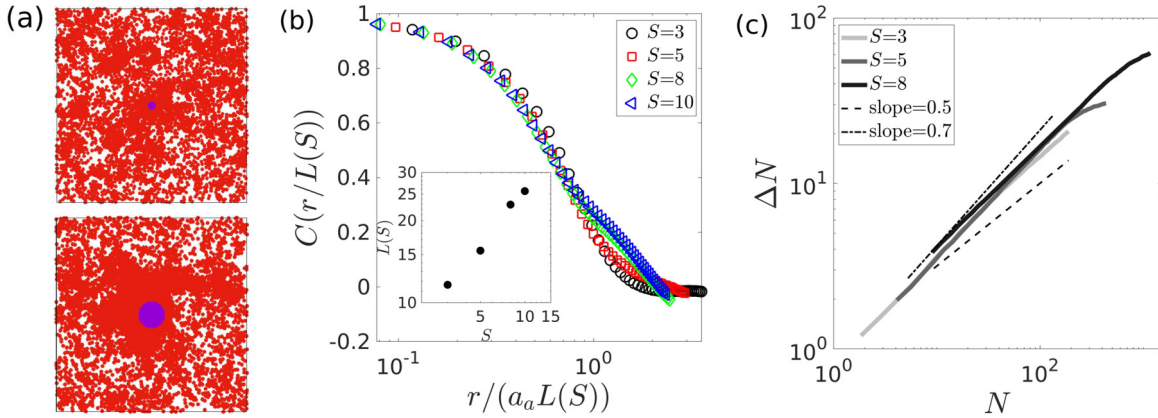
FIG. 5. (a) The top and bottom panels show instantaneous snapshots of the system for size ratios $S = 3$ and 8, respectively. Many such configurations are used to calculate the density correlations $C(r)$. Red particles are ABPs and the blue particle at the center is the bigger passive particle. (b) The main panel shows normalized correlations of density fluctuations $C(r)$ due to a passive particle for various size ratios S. The inset show the length scale extracted from $C(r)$ as a function of the size ratio. The length scale is expressed in terms of active particle size. (c) Number fluctuations of active particles around an isolated passive particle for three sizes S = 3, 5, and 8.

density fluctuations will influence the effective potential between passive particles. This notion is reminiscent of the role that concentration fluctuations play in the origin of critical Casimir forces in a binary mixture [59,60] and the density fluctuations of depletants that are responsible for depletion forces in colloid-polymer mixtures [47,48]. To highlight these aspects in our simulations, we consider a single passive particle in a system of ABPs. An instantaneous snapshot of the active particles and a passive particle is shown in the top and bottom panels of Fig. 5(a) for size ratios $S = 3$ and 8, respectively. The active particles cluster around the passive particle, and this clustering is enhanced for larger size ratios. This effect is elucidated by computing the time-averaged density correlation $C(r) = (\langle \rho(0)\rho(r) \rangle - \langle \rho(r) \rangle^2)/(\langle \rho(r)^2 \rangle - \langle \rho(r) \rangle^2)$ of active particles. The correlations are calculated by considering circular bins of width $dr = 0.5a_a$ around the particle center, starting from its surface. So, $\rho(0)$ is the average particle density in the first bin from the surface of the particle and $\rho(r)$ is the average particle density in a bin at a distance r from the surface with an area $2\pi r \, dr$. The scaled correlations $C[r/L(S)]$ corresponding to size ratios $S = 3, 5, 8$, and 10 are shown in Fig. 5(b). It is evident that the correlations show a good scaling with respect to the correlation length $L(S)$. The inset of Fig. 5(b) shows a correlation length $L(S)$ extracted from $C(r)$ to characterize the typical size of clusters; $L(S)$ is measured in terms of size of ABPs. Clearly, $L(S)$ increases linearly with S. Apparently, increasing the size ratio leads to a larger number of active particles interacting with a passive particle, so it promotes bigger clusters. Since the correlation $C(r)$ scales with $L(S)$, the relative size of the passive particle determines the density correlation of ABPs. These results strongly suggest that larger passive particles interact over longer distances due to enhanced density correlations of active particles.

The examination of number fluctuations ΔN of active particles around an isolated passive particle yields similar conclusions. It is computed considering an annular disk with inner radius equal to the radius of the passive particle and outer radius is varied. The mean and variance of the number of ABPs are calculated for the different outer radius of the

disk. The same is repeated for three different sizes of the passive particle or for three different size ratios $S = 3, 5$, and 8. In Fig. 5(c), we show the plot of ΔN vs N for three sizes $S = 3, 5$, and 8. For all the cases the graph is a power law with $\Delta N \simeq N^\alpha$, where $\alpha \simeq 0.7$ for moderate N for all S and starts to deviate for large N. The deviation appears at relatively larger N on increasing size ratio. Hence, increasing the size of the passive particle increases the stretch of density fluctuation of ABPs. These results establish that increasing the size ratio leads to longer density correlations that play a central role in the emergence of long-range effective potential between passive particles in our simulations.

The above results of the numerical simulation were obtained at a packing density of $\phi_a = 0.5$ of ABPs. Keeping in mind that experiments are performed at lower packing densities of bacteria, we present the snapshots of the configuration of ABPs around a single passive particle for a lower packing fraction of $\phi_a = 0.3$ in Fig. 7 in Appendix A. The corresponding videos SV2 and SV3 for $S = 3$ and 8 are provided as Supplemental Material [54]. The snapshots and videos suggest that the density correlations of ABPs increase with increasing size ratio S at lower packing fractions as well.

A similar analysis of density correlations $C(r)$ of bacteria in experiments reveals that they are suppressed (see Fig. 8 in Appendix B). In addition to activity, the interactions between colloidal particles are mediated by hydrodynamics due to the presence of a fluid medium. Earlier studies of active-passive matter have shown that hydrodynamic interactions play an important role in promoting clustering [61,62]. However, a comprehensive understanding of these aspects would necessitate further investigations that are deferred for future work.

C. Phase behavior of active-passive mixture

We elucidate the effect of the above effective potential on the full microscopic simulations of the active-passive mixture performed using Eqs. (1)–(3). We simulated the system for Pe = 25 and size ratios $S = 3, 5$, and 8, which are close to experimental values. In Fig. 6, the steady-state snapshots of passive (blue, bigger) and active (red, smaller) are shown
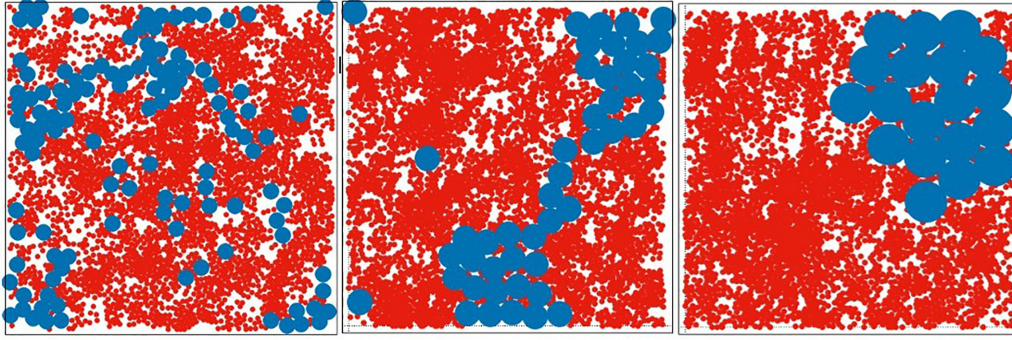
FIG. 6. Snapshots of the system obtained from the microscopic simulation: two types of particles for different size ratios $S = 3,\ 5,$ and 8 (left, central, and right columns) at Pe = 25. Red particles are ABPs and blue particles are passive particles, for fixed packing fraction $\phi = 0.60$ in a system of size $l_{\text{box}} = 140 a_a$.

for different size ratios $S = 3,\ 5,$ and 8 from left to right, respectively. Clusters with moderate to strong ordering are found on increasing S. For small $S = 3$, clusters are present but without strong local hexagonal ordering. As we increase S, the ordering and clustering is enhanced. We also calculated the percent of passive particles participating in the largest cluster for different size ratios and it increases from 35% to 67% as we increase size from 3 to 8 (data not shown). Hence for large size ratio passive particles show the macroscopic phase separation.

V. CONCLUSION

In summary, we have shown that the phase behavior of passive particles in active media is determined by the interplay of activity and the attractive effective potential of interaction. Our study establishes that the size ratio of passive to active particles provides a convenient way of tuning the effective potential to manipulate the nonequilibrium assembly of passive particles. When the size ratio is large, the effective potential is strong enough to lead to macroscopic phase separation of passive particles. Furthermore, our simulations have demonstrated that density fluctuations (correlations) of active particles play a key role in the origin of stronger effective potentials as the size ratio increases.

The colloidal particles in our experiments display dynamic clustering. However, the average size of clusters was observed to grow on increasing the size ratio [Fig. 3(b)]. This is because when the size of the colloidal particles is similar to that of bacteria, the clusters are disturbed easily by the bacteria. In contrast, the clusters of larger particles are relatively more stable. To understand these aspects in a better way, we performed simulations using a mixture of ABPs and passive particles. The effective potential between a pair of passive particles in active media was found to be attractive and dependent on the size ratio (Fig. 4). Increasing the size ratio made the effective potential stronger and long ranged. Further, our study suggests that the long-ranged interactions originate from enhanced density fluctuations of active particles around a passive particle. As the interactions of passive particles in our simulations are mediated by active particles, the density fluctuations of active particles have considerable influence on the nature of effective interactions between passive particles. The recent studies of a colloid-bacteria mixture had concluded that the torque on an active particle stabilizes the passive colloidal clusters [6]. Here, we provide an alternate view of the phenomenon based on effective potential that is intimately tied to density fluctuations of active particles.

The full simulations of active-passive mixtures showed that when the size ratio is small, the passive particles form dynamic clusters. However, when the size ratio is large, the effective interactions become strong enough to cause phase separation of colloidal particles. Even though our system displays many similarities with an equilibrium mixture
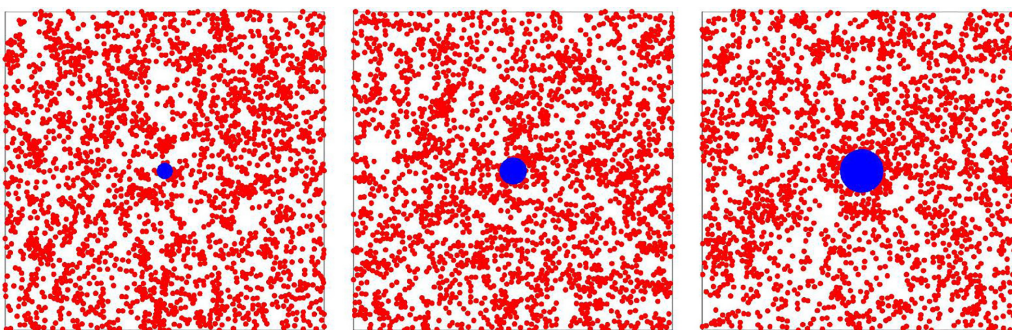

FIG. 7. Clustering of active particles in the presence of single passive particles at the center. Snapshots of the system for ABPs at packing fraction $\phi_a = 0.3$, for different size ratios $S = 3,\ 5,$ and 8, from left to right, respectively. The active particles are colored red and the centered blue particle is a passive particle.

of colloid-polymer, the underlying physics is strongly out of equilibrium. The simulations in our study have ignored the effect of hydrodynamic interactions. In experiments, the interactions between colloids are mediated by activity and hydrodynamics interactions. Exploring these aspects in detail will lead to a comprehensive understanding of active-passive mixtures.

APPENDIX A: DENSITY FLUCTUATIONS OF ACTIVE PARTICLES AT DILUTE DENSITIES

The packing density of active particles in Figs. 4 and 5 is $\phi_a = 0.5$. The density fluctuations of active particles observed in Fig. 5(a) persist even at lower packing densities. This is evident from the snapshots of active particles around a passive particle in Fig. 7 for $\phi_a = 0.3$ and $S = 3, 5,$ and 8.
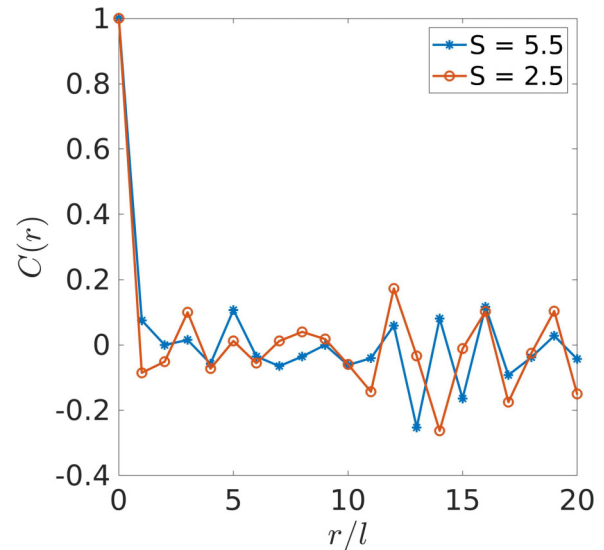

FIG. 8. The correlations of density fluctuations $C(r)$ of bacteria in experiments. It is shown for two different size ratios $S \sim 2.5$ and 5.5 of a colloidal particle. The x axis is scaled by the size of the bacteria l.

APPENDIX B: DENSITY FLUCTUATIONS OF BACTERIA AROUND AN ISOLATED COLLOIDAL PARTICLE

The time-averaged density correlations $C(r) = (\langle\rho(0)\rho(r)\rangle - \langle\rho(r)\rangle^2)/(\langle\rho(r)^2\rangle - \langle\rho(r)\rangle^2)$ are computed for bacteria around an isolated colloidal particle in experiments. These results are shown in Fig. 8 for size ratios $S = 2.5$ and 5.5, and they reveal that the density correlations are suppressed in our experiments.

[1] S. Sacanna, M. Korpics, K. Rodriguez, L. Colón-Meléndez, S.-H. Kim, D. J. Pine, and G.-R. Yi, Shaping colloids for self-assembly, Nat. Commun. **4**, 1688 (2013).

[2] T. Hueckel, G. M. Hocky, and S. Sacanna, Total synthesis of colloidal matter, Nat. Rev. Mater. **6**, 1053 (2021).

[3] S. Glotzer and M. Solomon, Anisotropy of building blocks and their assembly into complex structures, Nat. Mater. **6**, 557 (2007).

[4] P. N. Pusey, in *Liquids, Freezing and Glass Transition*, edited by J. P. Hansen, D. Levesque, and J. Zinn-Justin (North-Holland, Amsterdam, 1991), pp. 765–942.

[5] W. C. K. Poon, Colloidal suspensions, in *Oxford Handbook of Soft Condensed Matter*, edited by E. Terentjev and D. A. Weitz (Oxford University Press, Oxford, 2015), pp. 1–49.

[6] S. Gokhale, J. Li, A. Solon, J. Gore, and N. Fakhri, Dynamic clustering of passive colloids in dense suspensions of motile bacteria, Phys. Rev. E **105**, 054605 (2022).

[7] F. Kümmel, P. Shabestari, C. Lozano, G. Volpe, and C. Bechinger, Formation, compression and surface melting of colloidal clusters by active particles, Soft Matter **11**, 6187 (2015).

[8] P. Romanczuk, M. Bar, W. Ebeling, and B Lindner, Active Brownian particles, Eur. Phys. J.: Spec. Top. **202**, 1 (2012).

[9] S. Ramaswamy, Active matter, J. Stat. Mech.: Theory Exp. (2017) 054002.

[10] M. C. Marchetti, J.-F. Joanny, S. Ramaswamy, T. B. Liverpool, J. Prost, M. Rao, and R. A. Simha, Hydrodynamics of soft active matter, Rev. Mod. Phys. **85**, 1143 (2013).

[11] C. Bechinger, R. D. Leonardo, H. Lowen, C. Reichhardt, G. Volpe, and G. Volpe, Active particles in complex and crowded environments, Rev. Mod. Phys. **88**, 045006 (2016).

[12] T. Vicsek, A. Czirók, E. Ben-Jacob, I. Cohen, and O. Shochet, Novel Type of Phase Transition in a System of Self-Driven Particles, Phys. Rev. Lett. **75**, 1226 (1995).

[13] A. Bricard, J.-B. Caussin, N. Desreumaux, O. Dauchot, and D. Bartolo, Emergence of macroscopic directed motion in populations of motile colloids, Nature (London) **503**, 95 (2013).

[14] M. E. Cates and J. Tailleur, Motility-induced phase separation, Annu. Rev. Condens. Matter Phys. **6**, 219 (2015).

[15] I. Buttinoni, J. Bialké, F. Kümmel, H. Löwen, C. Bechinger, and T. Speck, Dynamical Clustering and Phase Separation in Suspensions of Self-Propelled Colloidal Particles, Phys. Rev. Lett. **110**, 238301 (2013).

[16] J. Palacci, S. Sacanna, A. P. Steinberg, D. J. Pine, and P. M. Chaikin, Living crystals of light-activated colloidal surfers, Science **339**, 936 (2013).

[17] H. H. Wensink, J. Dunkel, S. Heidenreich, K. Drescher, R. E. Goldstein, H. Löwen, and J. M. Yeomans, Meso-scale

turbulence in living fluids, Proc. Natl. Acad. Sci. USA **109**, 14308 (2012).

[18] H. M. Lopez, J. Gachelin, C. Douarche, H. Auradou, and E. Clement, Turning Bacteria Suspensions into Superfluids, Phys. Rev. Lett. **115**, 028301 (2015).

[19] X.-L. Wu and A. Libchaber, Particle Diffusion in a Quasi-Two-Dimensional Bacterial Bath, Phys. Rev. Lett. **84**, 3017 (2000).

[20] K. C. Leptos, J. S. Guasto, J. P. Gollub, A. I. Pesci, and R. E. Goldstein, Dynamics of Enhanced Tracer Diffusion in Suspensions of Swimming Eukaryotic Microorganisms, Phys. Rev. Lett. **103**, 198103 (2009).

[21] C. Valeriani, M. Li, J. Novosel, J. Arlt, and D. Marenduzzo, Colloids in a bacterial bath: Simulations and experiments, Soft Matter **7**, 5228 (2011).

[22] J.-L. Thiffeault, Distribution of particle displacements due to swimming microorganisms, Phys. Rev. E **92**, 023023 (2015).

[23] R. Jeanneret, D. O. Pushkin, V. Kantsler, and M. Polin, Entrainment dominates the interaction of microalgae with micron-sized objects, Nat. Commun. **7**, 12518 (2016).

[24] A. J. T. M. Mathijssen, R. Jeanneret, and M. Polin, Universal entrainment mechanism controls contact times with motile cells, Phys. Rev. Fluids **3**, 033103 (2018).

[25] H. Shum and J. M. Yeomans, Entrainment and scattering in microswimmer-colloid interactions, Phys. Rev. Fluids **2**, 113101 (2017).

[26] L. Ortlieb, S. Rafai, P. Peyla, C. Wagner, and T. John, Statistics of Colloidal Suspensions Stirred by Microswimmers, Phys. Rev. Lett. **122**, 148101 (2019).

[27] A. Lagarde, N. Dages, T. Nemoto, V. Demery, D. Bartolo, and T. Gibaud, Colloidal transport in bacteria suspensions: from bacteria collision to anomalous and enhanced diffusion, Soft Matter **16**, 7503 (2020).

[28] L. Angelani, C. Maggi, M. L. Bernardini, A. Rizzo, and R. Di Leonardo, Effective Interactions between Colloidal Particles Suspended in a Bath of Swimming Cells, Phys. Rev. Lett. **107**, 138302 (2011).

[29] D. Ray, C. Reichhardt, and C. J. Olson Reichhardt, Casimir effect in active matter systems, Phys. Rev. E **90**, 013019 (2014).

[30] R. Ni, M. A. Cohen Stuart, and P. G. Bolhuis, Tunable Long Range Forces Mediated by Self-Propelled Colloidal Hard Spheres, Phys. Rev. Lett. **114**, 018302 (2015).

[31] M. Zaeifi Yamchi and A. Naji, Effective interactions between inclusions in an active bath, J. Chem. Phys. **147**, 194901 (2017).

[32] F. Feng, T. Lei, and N. Zhao, Tunable depletion force in active and crowded environments, Phys. Rev. E **103**, 022604 (2021).

[33] F. Smallenburg and H. Löwen, Swim pressure on walls with curves and corners, Phys. Rev. E **92**, 032304 (2015).

[34] J. Harder, S. A. Mallorya, C. Tung, C. Valeriani, and A. Cacciuto, The role of particle shape in active depletion, J. Chem. Phys. **141**, 194901 (2014).

[35] P. Liu, S. Ye, F. Ye, K. Chen, and M. Yang, Constraint Dependence of Active Depletion Forces on Passive Particles, Phys. Rev. Lett. **124**, 158001 (2020).

[36] Y. Baek, A. P. Solon, X. Xu, N. Nikola, and Y. Kafri, Generic Long-Range Interactions Between Passive Bodies in an Active Fluid, Phys. Rev. Lett. **120**, 058002 (2018).

[37] A. K. Omar, Y. Wu, Z. G. Wang, and J. F. Brady, Swimming to stability: Structural and dynamical control via active doping, ACS Nano **13**, 560 (2019).

[38] S. R. McCandlish, A. Bhaskaran, and M. Hagan, Spontaneous segregation of self-propelled particles with different motilities, Soft Matter **8**, 2527 (2012).

[39] S. C. Takatori and J. F. Brady, A theory for the phase behavior of mixtures of active particles, Soft Matter **11**, 7920 (2015).

[40] J. Stenhammar, R. Wittkowski, D. Marenduzzo, and M. E. Cates, Activity-Induced Phase Separation and Self-Assembly in Mixtures of Active and Passive Particles, Phys. Rev. Lett. **114**, 018301 (2015).

[41] S. N. Weber, C. A. Weber, and E. Frey, Binary Mixtures of Particles with Different Diffusivities Demix, Phys. Rev. Lett. **116**, 058301 (2016).

[42] A. Wysocki, R. G. Winkler, and G. Gompper, Propagating interfaces in mixtures of active and passive Brownian particles, New J. Phys. **18**, 123030 (2016).

[43] P. Dolai, A. Simha, and S. Mishra, Phase separation in binary mixtures of active and passive particles, Soft Matter **14**, 6137 (2018).

[44] E. Ilker and J.-F. Joanny, Phase separation and nucleation in mixtures of particles with different temperatures, Phys. Rev. Res. **2**, 023200 (2020).

[45] F. Hauke, H. Lowen, and B. Liebchen, Clustering-induced velocity-reversals of active colloids mixed with passive particles, J. Chem. Phys. **152**, 014903 (2020).

[46] A. Y. Grosberg and J.-F. Joanny, Nonequilibrium statistical mechanics of mixtures of particles in contact with different thermostats, Phys. Rev. E **92**, 032118 (2015).

[47] S. Asakura and F. Oosawa, On interaction between two bodies immersed in a solution of macromolecules, J. Chem. Phys. **22**, 1255 (1954).

[48] H. N. W. Lekkerkerker, W. C. K. Poon, P. N. Pusey, A. Stroobants, and P. B. Warren, Phase behaviour of colloid + polymer mixtures, Europhys. Lett. **20**, 559 (1992).

[49] J. Adler and B. Templeton, The effect of environmental conditions on the motility of *Escherichia coli*, J. Gen. Microbiol. **46**, 175 (1967).

[50] R. L. Schilling and L. Partzsch, in *Brownian Motion:An Introduction to Stochastic Processes*, De Gruyter Textbook, contributed by B. Böttcher (De Gruyter Textbook, Berlin, 2012).

[51] Z. Schuss, *Brownian Dynamics at Boundaries and Interfaces: In Physics, Chemistry, and Biology* (Springer, New York, 2015).

[52] Y. Fily and M. C. Marchetti, Athermal Phase Separation of Self-Propelled Particles with No Alignment, Phys. Rev. Lett. **108**, 235702 (2012).

[53] A. Tiribocchi, R. Wittkowski, D. Marenduzzo, and M. E. Cates, Active Model H: Scalar Active Matter in a Momentum-Conserving Fluid, Phys. Rev. Lett. **115**, 188302 (2015).

[54] See Supplemental Material at http://link.aps.org/supplemental/10.1103/PhysRevE.108.034603 for videos of experiments and simulations.

[55] F. Peruani and M. Bär, A kinetic model and scaling properties of nonequilibrium clustering of self-propelled particles, New J. Phys. **15**, 065009 (2013).

[56] J. P. Singh, S. Pattanayak, S. Mishra, and J. Chakrabarti, Effective single component description of steady state structures of passive particles in an active bath, J. Chem. Phys. **156**, 214112 (2022).

[57] J. Dzubiella, J. Chakrabarti, and H. Lowen, Tuning colloidal interactions in subcritical solvents by solvophobicity:

Explicit versus implicit modeling, J. Chem. Phys. **131**, 044513 (2009).

[58] J. Chakrabarti, S. Chakrabarti, and H. Lown, Short ranged attraction and long ranged repulsion between two solute particles in a subcritical liquid solvent, J. Phys.: Condens. Matter **18**, L81 (2006).

[59] M. E. Fisher and P.-G. de Gennes, *Simple Views on Condensed Matter (3rd Edition)* (World Scientific, 2003), pp. 237–241.

[60] D. Bonn, J. Otwinowski, S. Sacanna, H. Guo, G. Weddam, and P. Schall, Direct Observation of Colloidal Aggregation by Critical Casimir Forces, Phys. Rev. Lett. **103**, 156101 (2009).

[61] A. S. Vishen, J. Prost, and M. Rao, Breakdown of effective temperature, power law interactions, and self-propulsion in a momentum-conserving active fluid, Phys. Rev. E **100**, 062602 (2019).

[62] R. C. Krafnick and A. E. Garcia, Impact of hydrodynamics on effective interactions in suspensions of active and passive matter, Phys. Rev. E **91**, 022308 (2015).